nature catalysis

The atomic-resolution crystal structure of activated [Fe]-hydrogenase

Gangfeng Huang[1,8], Tristan Wagner[1,7,8], Matthew D. Wodrich [2,3], Kenichi Ataka[4], Eckhard Bill[5], Ulrich Ermler[6], Xile Hu [2] and Seigo Shima [1]*

Hydrogenases are promising templates for constructing new H_2-based catalysts. [Fe]-hydrogenase, which features an iron-guanylylpyridinol (FeGP) cofactor, catalyses a reversible hydride transfer from H_2 to methenyl-tetrahydromethanopterin (methenyl-H_4MPT^+, a C_1 carrier in methanogens). Here, we present a detailed mechanistic scenario of this reaction based on the 1.06 Å resolution structure of [Fe]-hydrogenase in a closed active form, in which the Fe of the FeGP cofactor is positioned near the hydride-accepting C14a of a remarkably distorted methenyl-H_4MPT^+. The open-to-closed transition generates an unsaturated pentacoordinated Fe on expulsion of a water ligand. Quantum mechanics/molecular mechanics computations based on experimental models indicate that a deprotonated 2-OH group on the FeGP cofactor acts as a catalytic base and provides a fairly complete picture of H_2 activation: H_2 binding on the empty Fe site was found to be nearly thermo-neutral while H_2 cleavage and hydride transfer proceed smoothly. The overall reaction involves a repositioning and relaxation of the distorted methenyl-H_4MPT^+.

Hydrogenases are microbial enzymes that catalyse the consumption and production of H_2 and are excellent templates for designing H_2-activating mimetic catalysts[1–3]. Based on the metal composition of the active centre, these enzymes are classified into [NiFe]-, [FeFe]- and [Fe]-hydrogenases[4]. Among these, [Fe]-hydrogenase catalyses a reversible hydride transfer from H_2 to methenyl-tetrahydromethanopterin (methenyl-H_4MPT^+) to form methylene-H_4MPT (Fig. 1a)[5] and contains an iron-guanylylpyridinol (FeGP) cofactor as a prosthetic group (Fig. 1b)[6]. [Fe]-hydrogenase also catalyses proton exchange (H_2/D^+, $H_2/2D^+$) and *para/ortho*-H_2 exchange reactions only in the presence of methenyl-H_4MPT^+ (refs. [7–9]) and an exchange of the hydrogen atom in the *pro-R* position of methylene-H_4MPT with the protons of water[10].

Architecturally, [Fe]-hydrogenase is a homodimer built from two N-terminal domains and one central domain, where the latter is composed of the C-terminal segments from both monomers[11,12]. The N-terminal and central domains form two active-site clefts, with each serving as a binding site for the FeGP cofactor and the substrate (methenyl-H_4MPT^+/methylene-H_4MPT)[12–14]. The active-site clefts are predicted to adopt open and closed conformations. So far, the holoenzyme (bound with the FeGP cofactor) without a substrate[12,13] and the catalytically inactive C176A mutated holoenzyme complexed with methylene-H_4MPT[14] have only been structurally analysed in their open conformations. A catalytically irrelevant closed conformation was only found in the structure of the apoenzyme (with neither the FeGP cofactor nor the substrate bound)[11].

The [Fe]-centre of the FeGP cofactor has been identified as a key player for H_2 activation. Its low-spin Fe(II) is hexacoordinated with two CO, one pyridinol nitrogen, one acyl carbon, one cysteine thiolate and a wate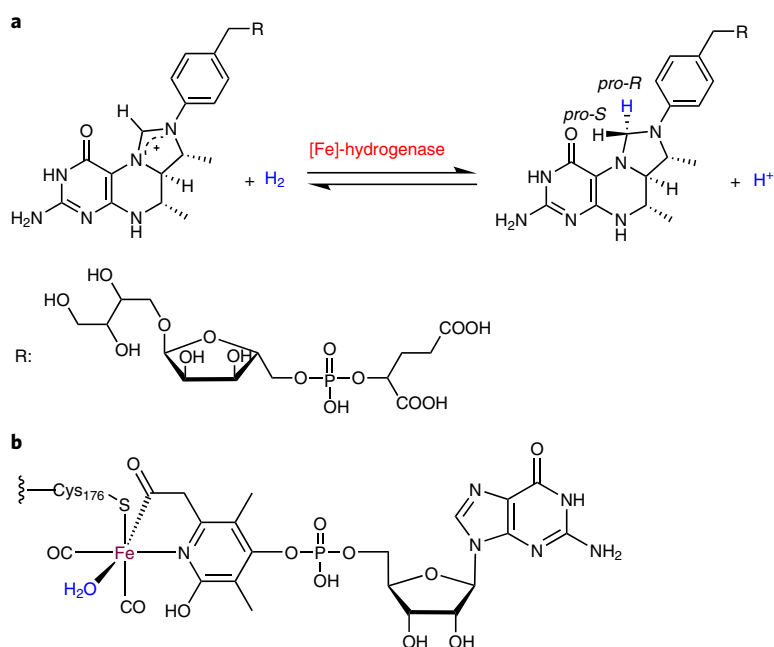r molecule in the open-inactive state of this enzyme (Fig. 1b)[13]. The water-binding site of Fe has been predicted to be the site of H_2 binding based on spectroscopic and structural analyses of [Fe]-hydrogenase complexed with inhibitors[14–17]. Using these data, various density functional theory (DFT) based computational studies have been performed and catalytic mechanisms proposed[14,18–20]. Even before the discovery of the FeGP cofactor, a catalytic mechanism involving a C14a carbocation adjusted by a specific protein surrounding was proposed, in which H_2 was bound to C14a and then heterolytically cleaved in a reaction similar to that of alkanes and H_2 under superacid conditions[7,9,21,22]. Despite considerable effort, the reaction mechanism of [Fe]-hydrogenase remains obscure, primarily because of the lack of information about the closed active conformation. In particular, a [Fe]-hydrogenase–methenyl-H_4MPT^+ complex structure is indispensable.

Here, we present an atomic-resolution crystal structure (1.06 Å resolution) of a substrate-bound closed active form. Based on the structural and quantum mechanics/molecular mechanics (QM/MM) data, we present a fairly precise catalytic scenario for the [Fe]-hydrogenase reaction.

Results

Structures of [Fe]-hydrogenase in the open/closed states. Crystal structures were determined for the [Fe]-hydrogenase holoenzyme from *Methanococcus aeolicus* in an open state at 2.3 Å resolution (PDB code 6HAC), which essentially corresponds to that previously reported (Fig. 2a) and for the [Fe]-hydrogenase holoenzyme–methenyl-H_4MPT^+ complex in a closed state at 1.06 Å (crystal form A, PDB code 6HAV) and 1.85 Å (form B, PDB code 6HAE) resolution (Fig. 2b and Supplementary Table 1). The crystals containing the enzyme in the open state were obtained in the absence of the

Fig. 1 | The catalytic reaction and chemical structures. a, [Fe]-hydrogenase reversibly catalyses the reduction of methenyl-H_4MPT^+ with H_2 (ref. [5]). For computations, the tail 'R' was truncated and the molecules termed MPT^+ (oxidized) and HMPT (reduced). **b**, The chemical structure of the FeGP cofactor of [Fe]-hydrogenase in the open form[6].

substrates under 95%N_2/5%H_2, whereas crystals in the closed state grew only in the presence of methenyl-H_4MPT^+ under 100% N_2. The trick for crystallization in the absence of H_2 was to suppress the catalytic cycling from the open into the closed state and vice versa. The structures of the N-terminal and central domains were nearly identical in the two states (open and closed) (Fig. 2a,b), which indicates a rigid body movement of the N-terminal domains in the open/closed conformational changes (Supplementary Fig. 1).

The X-ray structures of the closed states of [Fe]-hydrogenase show the FeGP cofactor and methenyl-H_4MPT^+ embedded in the cleft walls of the N-terminal and central domains, respectively (Fig. 2b). In contrast to their separate positions in the open state[14], the FeGP cofactor and substrate of the closed [Fe]-hydrogenase are proximate to one another and form multiple contacts (Fig. 2b,d,e). His14 and Trp148 are oriented with their bulky side chains towards the Fe centre and Met252, Met321' and Phe281' (amino-acid residues of the partner monomer are marked with a prime) towards methenyl-H_4MPT^+ to clamp the rings together and to adjust the ring conformations for creating a proper active-site geometry. The most pronounced residue, Met252, provides van der Waals contacts between its sulfur and C14a of methenyl-H_4MPT^+ as well as between its methyl group and the phenyl ring of methenyl-H_4MPT^+ (Fig. 2e and Supplementary Fig. 2). The important function of Met252 in catalysis is substantiated by its strict conservation in [Fe]-hydrogenases (Supplementary Fig. 3) and the dramatic decrease of the specific activity measured for the Met252 to alanine, serine and phenylalanine variants (Supplementary Table 2).

The tight packing in the closed conformation causes a tilt of the pyridinol ring of the FeGP cofactor of 15° (Supplementary Fig. 4) and of the imidazoline and phenyl rings of methenyl-H_4MPT^+ of ~20° compared to their orientations in the open methylene-H_4MPT-bound C176A holoenzyme variant. As a first consequence, the distance between His14 and the 2-OH of the pyridinol is shortened from 4.9 Å to 3.3 Å, which makes the latter a part of a proton relay, as shown in Supplementary Fig. 5. The shorter distance causes a pK_a decrease of the 2-OH group in the closed state and

corroborate its dedicated role as a catalytic base in the enolate form during H_2 cleavage. As a second consequence, the tilt of the imidazoline ring of methenyl-H_4MPT^+ towards the Fe centre reduces the distance between Fe and C14a to 3.8 Å, which agrees with the range of distances for H_2 activation predicted by previous DFT computations[19,20]. The water ligand of Fe thereby becomes dissociated (Fig. 2c,d), as predicted by Dey[18].

Despite encapsulation of the catalytic part of the bulky FeGP cofactor and the substrate upon cleft closure, the Fe centre is still accessible by a narrow hydrophobic channel most likely used by H_2 (Supplementary Fig. 6). In the channel of crystal form A, but not in one monomer of form B, a weak elongated electron density is visible reaching the unoccupied Fe(II) binding site. Obviously, linear and rather hydrophobic compounds like O_2, N_2 or HSCN can bind with a low occupancy in the absence of H_2. The modelling of two water molecules did not adequately explain the elongated shape of the electron density (their occupancy was only 40–50%; Supplementary Fig. 7).

Spectroscopic analyses. A Mössbauer spectrum of [Fe]-hydrogenase from *M. aeolicus* in aqueous solution revealed two species whose iron sites have slightly different electronic structures (Supplementary Fig. 8). The dominant species, subspectrum 2 (80% relative intensity), was similar to that of [Fe]-hydrogenase purified from *Methanothermobacter marburgensis*[23], while subspectrum 1 was not visible in previous experiments[23,24]. On adding methenyl-H_4MPT^+ to *M. aeolicus* [Fe]-hydrogenase, subspectrum 1 increased, such that both species had nearly the same intensity (55:45). Mössbauer subspectra 1 and 2 differ mainly by the isomer shift of 0 versus 0.09 mm·s^{-1}. The higher isomer shift of subspectrum 2 most probably corresponds to hexa-coordination of Fe in the open form, whereas penta-coordination of Fe in the closed state leads, on average, to shortened bonds and thus lower isomer shifts[25]. Therefore, Mössbauer spectra 1 and 2 presumably reflect closed and open conformations of the enzyme, respectively.

Moreover, infrared spectroscopic data indicated that the relative intensities and frequencies of the asymmetric CO (~2,000 cm^{-1}) and
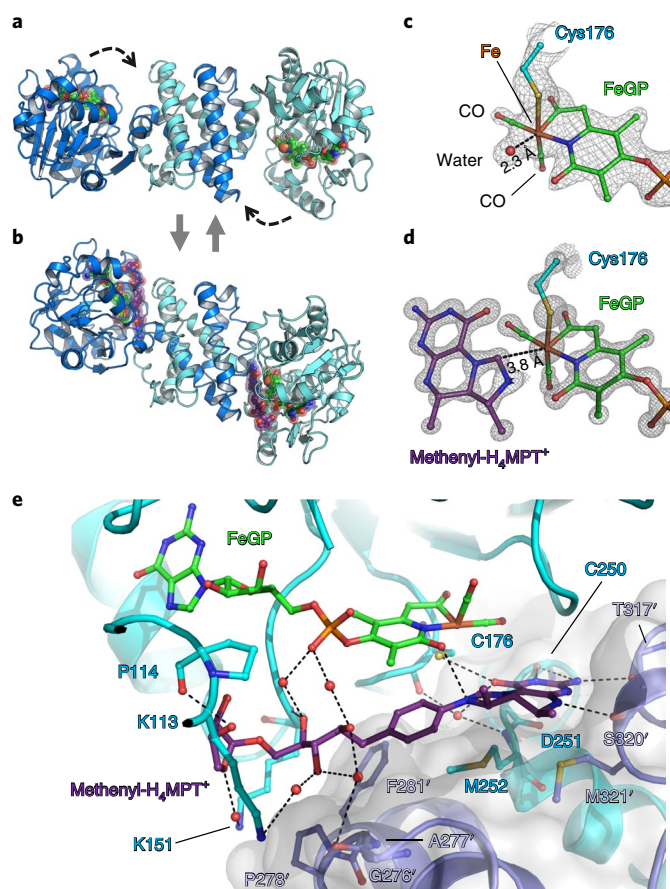
Fig. 2 | Structures of the open and closed conformations of [Fe]-hydrogenase. a, The open conformation of [Fe]-hydrogenase without substrate at 2.3 Å resolution. The curved and dashed arrows indicate the movement of the N-terminal domains. **b**, The closed conformation of [Fe]-hydrogenase with methenyl-H_4MPT^+ bound at 1.06 Å resolution. The two monomers are shown in cartoon models and coloured in blue and light blue. Methenyl-H_4MPT^+ (carbon in purple) and the FeGP cofactor (carbon in green) are shown as sticks, with nitrogen, oxygen, phosphorous, sulfur and Fe atoms coloured in dark blue, red, orange, yellow and light brown, respectively. **c**, The structure of the FeGP cofactor at the active site in the open conformation. The $2F_o$–F_c electron density map is shown as a mesh (contoured at 2.0 σ). **d**, The structures of the FeGP cofactor and methenyl-H_4MPT^+ in the active site cleft of [Fe]-hydrogenase in the closed conformation. The $2F_o$–F_c electron density map is shown as meshes (contoured at 3.0 σ). **e**, A close-up view of the active site of closed [Fe]-hydrogenase in complex with the FeGP cofactor (carbons in green) and methenyl-H_4MPT^+ (carbons in purple). The two monomers are depicted as light blue and light purple cartoon models. The amino-acid residues of the partner monomer are marked with a prime.

symmetric CO (~1,940 cm^{-1}) bands are almost unchanged in the absence and presence of methenyl-H_4MPT^+ (Supplementary Fig. 9). Thus, the geometry of the CO ligands and presumably of the entire Fe centre appears to be largely maintained when switching from the hexa- to the pentacoordinated Fe upon H_2O removal.

Structures of the FeGP cofactor and methenyl-H_4MPT^+. The 1.06 Å electron-density map of closed [Fe]-hydrogenase allows for an accurate analysis of the geometric parameters of the FeGP cofactor and methenyl-H_4MPT^+ (Fig. 3). The planarity of the pyridinol/pyridone ring of the FeGP cofactor and the C2–O distance of 1.33 Å (for reference, C–O single bond of phenol, 1.36 Å; C=O
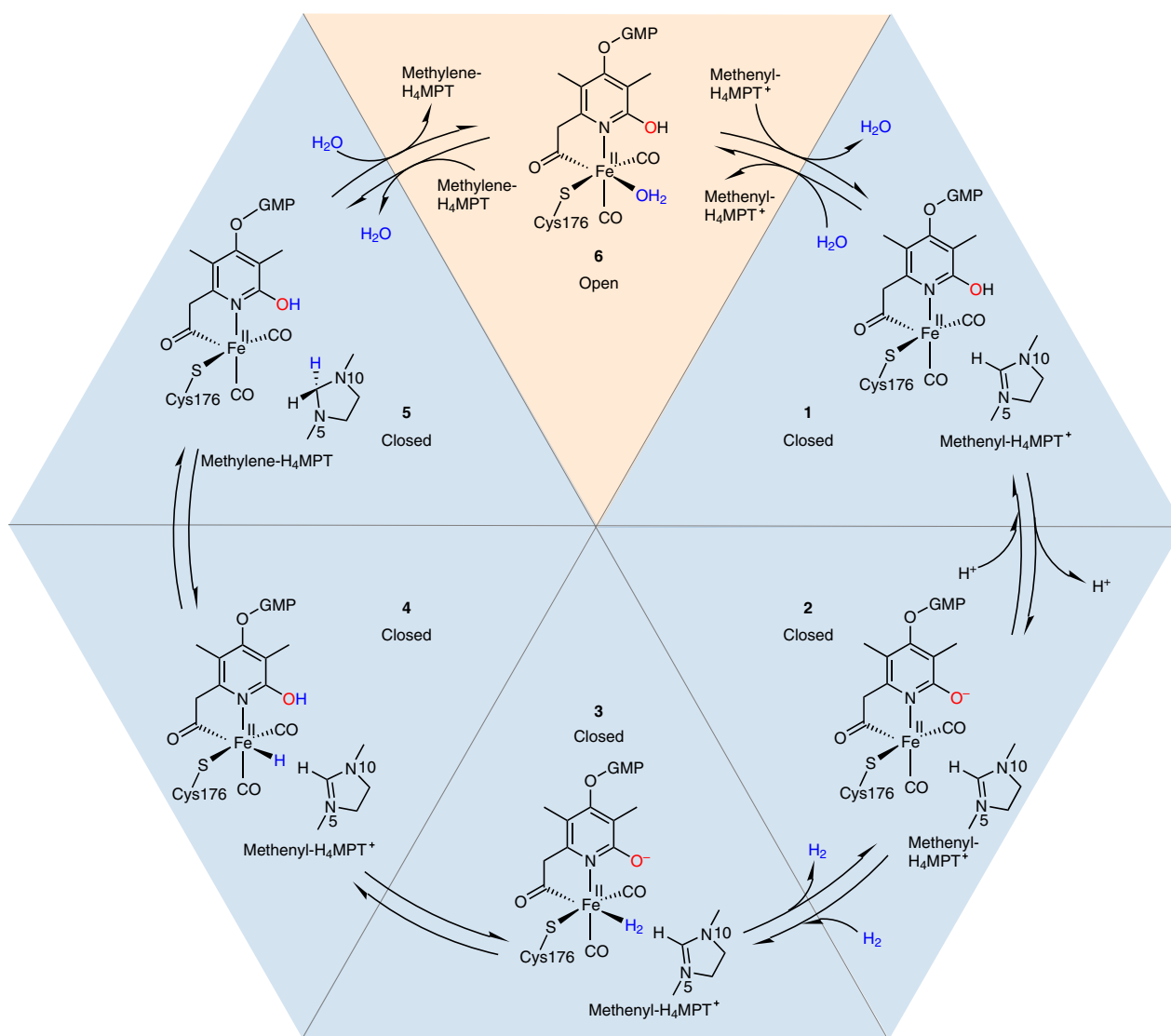
double bond within an aromatic ring, 1.2 Å) support an enol or enolate tautomeric state with the 2-OH group serving as the catalytic base. A distinction between enol and enolate forms is not possible. The bond distances and angles of the FeGP cofactor are very similar to those of a mimetic compound with pentacoordinated iron (Supplementary Fig. 10)[26].

Substantial deviations from the standard geometry are identified in the imidazoline of the pterin-imidazoline-phenyl ring system of methenyl-H_4MPT^+. The distance of 1.23 Å between N5 and C14a is substantially shorter (Fig. 3c,d and Supplementary Fig. 11) than that of the relaxed state (1.31 Å). Consistently, the distance of the C14a–N10 bond (1.43 Å) is longer than in the relaxed state (1.33 Å). As a consequence, the positive charge on N5 and the negative charge on N10 are increased in a distorted conformation compared to a fully relaxed one, while the charge on C14a is unchanged (Supplementary Fig. 12). N5 may stabilize the electron-rich Fe–H intermediate that is generated during H_2 cleavage. The short C=N double bond of the imidazoline ring as well as the lack of a hydrogen bond donor to the lone-pair electron of N5 and N10 and an acidic amino acid to C14a do not coincide with C14a being a carbocation, as previously proposed[9,21,22]. Notably, the firmly fixed polypeptide surrounding of the substrate appears to enforce the tilt of the phenyl ring out of the plane formed with C14a, N5 and N10, which increases the sp^3 character of N10 and may cause the observed distorted imidazoline geometry. The partial negative charge on N10 might increase the pK_a of the 2-OH of the FeGP cofactor, which stabilizes its protonated state (N10–2OH distance, 3.08 Å).

Catalytic mechanism. To better understand the catalytic mechanism of [Fe]-hydrogenase, we studied the processes that occur in the closed conformation of the enzyme (Fig. 4) using QM/MM based on the ONIOM method (see Methods for computational details). The QM/MM computations revealed a protonated imidazole group of His14 and a deprotonated 2-OH group of pyridinol to be a local minimum. The free energy profile of the catalytic cycle indicates an overall facile process (Supplementary Figs. 13 and 14). Starting with a deprotonated 2-OH group of the pyridinol (which can serve as a catalytic base for H_2 activation[20,27]) located on the FeGP cofactor (**2**), the binding of H_2 onto the empty sixth coordination site of the Fe centre (**2→3**) is very mildly exergonic (−0.2 kcal mol^{-1}). H_2 can then be heterolytically cleaved between the proximate O$^-$ (which accepts the proton) and the Fe centre (which retains the hydride anion) with a low barrier of only 7.8 kcal mol^{-1} (**3 → TS3,4**). The resulting intermediate, **4**, is stabilized by 8.9 kcal mol^{-1} relative to the transition state. A second energetic barrier is encountered during the transfer of the hydride anion from Fe to C14a located on the MPT$^+$ substrate (**4 → TS4,5**), which is lower than that involved in heterolytic H_2 cleavage (5.8 versus 7.8 kcal mol^{-1}) according to our computations. The resulting intermediate (**5**) is then stabilized by 7.7 kcal mol^{-1} relative to the transition state. From here, the enzyme would switch back to the open conformation (**5→6**), where a water molecule coordinates to the empty sixth ligation site of Fe.

One interesting feature is that the crystal structure shows a considerable distance between the Fe centre and the C14a atom of the MPT$^+$ substrate. However, during the course of optimization of the active site, our computations revealed that a considerable amount of volume is available and that the MPT$^+$ substrate is sufficiently flexible to allow movement closer to the Fe centre during the catalytic process. For example, the Fe⋯C14a distance decreases from 3.73 Å (**4**) to 3.34 Å (**TS4,5**) to 3.21 Å (**5**) over the course of the catalytic mechanism (Supplementary Fig. 15), which presumably greatly reduces the energetic cost associated with the hydride transfer process. Moreover, our computations show that the aforementioned distortion of the imidazoline ring is alleviated in the computed models (Supplementary Fig. 15), where the N5–C14a and C14a–N10 bond lengths (that is, 1.33 Å and 1.32 Å in **2**) closely match those

Fig. 3 | Electron density map and model of the cofactor and substrate. a–d, FeGP cofactor (**a,b**) and methenyl-H$_4$MPT$^+$ (**c,d**) in the closed state of [Fe]-hydrogenase from *M. aeolicus* at 1.06 Å resolution. The 2F_o-F_c electron density map of the FeGP cofactor (**a**) and methenyl-H$_4$MPT$^+$ (**c**) are shown as meshes (contoured at 4.0 σ) with orange surfaces (contoured at 5.2 σ). The FeGP cofactor and methenyl-H$_4$MPT$^+$ are shown as ball-and-stick models. Bond lengths are shown between the atoms of the FeGP cofactor (**b**) and methenyl-H$_4$MPT$^+$ (**d**). Carbon, nitrogen, oxygen, phosphorous, sulfur and iron atoms are depicted as green, dark blue, red, orange, yellow and light brown spheres, respectively.

of a free MPT$^+$ substrate (1.31 Å and 1.33 Å). More typical bond lengths are seen in other structures (for example, **4** and **5**). Taken together, these data further indicate that the active site contains enough free volume for the MPT$^+$ substrate to reorient itself to facilitate hydride transfer. Overall, our computations reveal that the catalytic process should occur very quickly in the enzyme's closed conformation. Note, however, that these computations cannot exclude the presence of the distorted methenyl-H$_4$MPT$^+$ observed in the closed crystal, because changes to the size of the QM region of the active site and the presence of the second monomer (which was excluded in our computations) may subtly influence the geometry of the active site. The presence of a distorted methenyl-H$_4$MPT$^+$ might further decrease the activation energy of heterolytic H$_2$ cleavage (**TS3,4**).

Conclusions

In summary, based on both the new crystal structures and QM/MM computations, we propose a catalytic cycle for [Fe]-hydrogenase (Fig. 4). In contrast to [NiFe]- and [FeFe]-hydrogenases, [Fe]-hydrogenase reveals, as a central feature, conversion between the open substrate-accessible and the closed catalytically active forms (Supplementary Video 1). The tightly associated FeGP-cofactor/substrate pair in the closed state expels a water ligand from the saturated hexacoordinated Fe, which allows thermo-neutral binding of H$_2$ to the moderately polar and unsaturated site of the Fe centre (which can be accessed via a narrow channel). Methenyl-H$_4$MPT$^+$ not only serves as a hydride acceptor but also plays a key role in tuning the iron centre for H$_2$-binding/activation. Activation of the active site by removal of the water ligand by substrate binding answers the long-standing question concerning the reasons for the substrate dependence of the proton-exchange reaction of [Fe]-hydrogenase[7,9,18]. The overall reaction appears to include repositioning and relaxing of the distorted substrate, as shown by QM/MM computations (Fig. 4). The catalytic-site structure of [Fe]-hydrogenase and the H$_2$-based hydrogenation process offer a strong basis for developing new synthetic and plastic catalysts that catalyse the hydrogenation of novel substrates with H$_2$.

Methods

Crystallization of the [Fe]-hydrogenase from *M. aeolicus*. Substrate-free [Fe]-hydrogenase holoenzyme from *M. aeolicus* was crystallized in an anaerobic tent with gas composition of 95%N$_2$/5%H$_2$ at 8 °C by using the sitting drop vapour diffusion method using 96-well two-drop MRC crystallization plates (Molecular Dimensions). For the initial screening, 0.7 µl of 24 mg ml^{-1} reconstituted [Fe]-hydrogenase was mixed with 0.7 µl of reservoir solution (of crystallization kits) under yellow light and incubated under dark conditions. The best diffracting diamond-shaped crystal grew in one month with 20% wt/vol polyethylene glycol 3350, 100 mM tri-sodium citrate pH 4.0 and 200 mM tri-sodium citrate as reservoir solution (JBScreen Wizard 3 & 4 HTS screening kit, Jena Bioscience). Crystallization of [Fe]-hydrogenase–methenyl-H$_4$MPT$^+$ complex was performed in the anaerobic tent with gas-phase 100%N$_2$ at room temperature under dark conditions. [Fe]-hydrogenase holoenzyme (50 mg ml^{-1}) was mixed with 10 mM methenyl-H$_4$MPT$^+$, both dissolved in 10 mM 3-(N-morpholino)propanesulfonic acid/KOH pH 7.0. The final concentrations of [Fe]-hydrogenase and methenyl-H$_4$MPT$^+$ were 24 mg ml^{-1} and 3 mM, respectively. After incubating the mixture in this tent under dark conditions for 5 min, the enzyme solution was centrifuged using a MiniSpin-plus system (Eppendorf) at 8,000 r.p.m. for 5 min using

Fig. 4 | The proposed catalytic cycle of [Fe]-hydrogenase. The open and closed forms are highlighted by the light orange and light blue backgrounds, respectively. Following the binding of methenyl-H_4MPT^+ and closure of the active-site cleft, the water molecule on the Fe site is removed. The distorted methenyl-H_4MPT^+ was observed in the crystal structure of the closed state (step 1 or 2). H_2 is bound to the open Fe site (step 3) and then heterolytically cleaved (step 4). Subsequently, the hydride on the Fe site is transferred to C14a of methenyl-H_4MPT^+ in a stereospecific manner (*pro-R* position) to generate methylene-H_4MPT (step 5).

centrifugal filters (0.45 μm) made of polyvinylidene fluoride (Millipore) to remove the aggregated proteins and dusts. After mixing 0.7 μl drop and 0.7 μl reservoir solution spotted on 96-well MRC crystallization plates (Molecular Dimensions), crystals emerged with the JBScreen Wizard 3 & 4 HTS (Jena Bioscience) kit containing 20% wt/vol polyethylene glycol 3350 and 200 mM sodium thiocyanate. For reproduction, the crystallization solution of the company was essential. The best diffracting long rod-shaped crystal belonging to form A was obtained in two weeks in a protein-mixture-to-crystallization-reservoir ratio of 2 μl:2 μl spotted on a 24-well Junior Clover plate. The plate-shaped crystals belonging to form B grew under the same crystallization conditions supplemented by 3% wt/vol 1,5-diaminopentane dihydrochloride with a ratio of 0.7 μl protein mixture to 0.7 μl crystallization reservoir (in 96-well plates).

Structural analysis. Crystals of the substrate-free [Fe]-hydrogenase holoenzyme from *M. aeolicus* were flash-frozen (3–5 s) in a solution containing 20% wt/vol polyethylene glycol 3350, 100 mM tri-sodium citrate pH 4.0, 200 mM tri-sodium citrate and 10% vol/vol glycerol at 8 °C in an anaerobic tent (with a gas composition of 95% N_2/5% H_2). Crystals of forms A and B from the co-crystallization of reconstituted [Fe]-hydrogenase and methylene-H_4MPT^+ were flash-frozen in the anaerobic tent (100% N_2) in their respective crystallization solution supplemented with 20% vol/vol glycerol. The diffraction experiments for substrate-free

[Fe]-hydrogenase were performed at 100 K on beamline BM30A (French Beamline for Investigation of Proteins) at the European Synchrotron Radiation Facility (ESRF) equipped with an ADSC Q315r charge-coupled device detector. The best data for form A and B crystals were collected at beamline PXII at the Swiss Light Source equipped with a PILATUS 6M detector. The data were processed with XDS[28] and scaled with SCALA from the CCP4 suite[29].

The structure of substrate-free [Fe]-hydrogenase was determined by molecular replacement with PHASER[30] by using the native [Fe]-hydrogenase from *M. marburgensis* in complex with 2-naphthylisocyanide (PDB:4JJF) as a template. The structures of forms A and B were solved with PHASER by using the first structure of the reconstituted [Fe]-hydrogenase from *M. aeolicus*. The N- and C-terminal domains were separately used as templates for the molecular replacement. The models were manually built with COOT[31] and refined with BUSTER[32] for the substrate-free and form B substrate-bound [Fe]-hydrogenase structure. Form A [Fe]-hydrogenase was refined with Phenix[33] considering all atoms except water as anisotropic and by adding the hydrogens in the riding position. The final models were validated using the MolProbity server (http://molprobity.biochem.duke.edu)[34]. Data collection, refinement statistics and PDB code for the deposited model are listed in Supplementary Table 1. The hydrogens were omitted in the final deposited model. The figures were generated and rendered with PyMOL (version 1.7, Schrödinger).

Conformational change of [Fe]-hydrogenase. The transformation from the experimentally obtained open form to closed form was calculated with the morphing option from the Morph Server6[35]. In the open form, methenyl-H_4MPT^+ is modelled into the central domain as observed in the closed form (Supplementary Video 1).

QM/MM computations. To assess the free energies associated with the portion of the catalytic cycle that occurs in the closed enzyme conformation (Fig. 4), we used QM/MM computations within the ONIOM (ref. [36]) framework in Gaussian09 (ref. [37]). An active site consisting of truncated versions of the FeGP cofactor and the substrate (MPT$^+$), as well as Cys176 and the proton transfer network (His14, Glu207, Thr20, Arg101 and two water molecules), shown in Supplementary Fig. 5, were included in the 'high level' computations at the M06/6-31G(d.p) level (ref. [38,39]). The 'low level' (computed using the universal force field) included the remaining portions of the truncated FeGP cofactor and MPT$^+$ substrate, as well as all other amino-acid residues of a single monomer. Amino acids with electrically charged subgroups were protonated or deprotonated according to a physiological pH, which produced an overall charge of −13 for the protein (neutral for the high level/−13 for the low level). The nature of all stationary points (as either minima or transition states) was confirmed by analysis of vibrational frequencies (zero for minima, one for transition states). Reported free energies include unscaled free energy contributions taken from the QM/MM computations. The atomic coordinates of the optimized computational models (steps 2–5, **TS3,4** and **TS4,5**) are available as Supplementary Data 1–6.

Reporting Summary. Further information on research design is available in the Nature Research Reporting Summary linked to this article.

Data availability
The data that support the plots within this paper and other findings of this study are available from the corresponding authors on reasonable request. X-ray crystallographic data are available in the RCSB-Protein Data Bank under accession numbers 6HAC (open conformation), 6HAV (closed conformation form A) and 6HAE (closed conformation form B).

References
1. Fontecilla-Camps, J. C., Volbeda, A., Cavazza, C. & Nicolet, Y. Structure/function relationships of [NiFe]- and [FeFe]-hydrogenases. *Chem. Rev.* **107**, 4273–4303 (2007).
2. Lubitz, W., Ogata, H., Rudiger, O. & Reijerse, E. Hydrogenases. *Chem. Rev.* **114**, 4081–4148 (2014).
3. Thauer, R. K. et al. Hydrogenases from methanogenic archaea, nickel, a novel cofactor and H_2 storage. *Annu. Rev. Biochem.* **79**, 507–536 (2010).
4. Vignais, P. M. & Billoud, B. Occurrence, classification and biological function of hydrogenases: an overview. *Chem. Rev.* **107**, 4206–4272 (2007).
5. Zirngibl, C. et al. H_2-forming methylenetetrahydromethanopterin dehydrogenase, a novel type of hydrogenase without iron–sulfur clusters in methanogenic archaea. *Eur. J. Biochem.* **208**, 511–520 (1992).
6. Shima, S. & Ermler, U. Structure and function of [Fe]-hydrogenase and its iron-guanylylpyridinol (FeGP) cofactor. *Eur. J. Inorg. Chem.* **2011**, 963–972 (2011).
7. Vogt, S., Lyon, E. J., Shima, S. & Thauer, R. K. The exchange activities of [Fe] hydrogenase (iron–sulfur-cluster-free hydrogenase) from methanogenic archaea in comparison with the exchange activities of [FeFe] and [NiFe] hydrogenases. *J. Biol. Inorg. Chem.* **13**, 97–106 (2008).
8. Hartmann, G. C., Santamaria, E., Fernández, V. M. & Thauer, R. K. Studies on the catalytic mechanism of H_2-forming methylenetetrahydromethanopterin dehydrogenase: *para-ortho* H_2 conversion rates in H_2O and D_2O. *J. Biol. Inorg. Chem.* **1**, 446–450 (1996).
9. Thauer, R. K., Klein, A. R. & Hartmann, G. C. Reactions with molecular hydrogen in microorganisms: evidence for a purely organic hydrogenation catalyst. *Chem. Rev.* **96**, 3031–3042 (1996).
10. Schleucher, J., Schwörer, B., Thauer, R. K. & Griesinger, C. Elucidation of the stereochemical course of chemical reactions by magnetic labeling. *J. Am. Chem. Soc.* **117**, 2941–2942 (1995).
11. Pilak, O. et al. The crystal structure of the apoenzyme of the iron–sulfur cluster-free hydrogenase. *J. Mol. Biol.* **358**, 798–809 (2006).
12. Shima, S. et al. The crystal structure of [Fe]-hydrogenase reveals the geometry of the active site. *Science* **321**, 572–575 (2008).
13. Hiromoto, T. et al. The crystal structure of C176A mutated [Fe]-hydrogenase suggests an acyl–iron ligation in the active site iron complex. *FEBS Lett.* **583**, 585–590 (2009).
14. Hiromoto, T., Warkentin, E., Moll, J., Ermler, U. & Shima, S. The crystal structure of an [Fe]-hydrogenase-substrate complex reveals the framework for H_2 activation. *Angew. Chem. Int. Ed.* **48**, 6457–6460 (2009).
15. Lyon, E. J. et al. Carbon monoxide as an intrinsic ligand to iron in the active site of the iron–sulfur-cluster-free hydrogenase H_2-forming methylenetetrahydromethanopterin dehydrogenase as revealed by infrared spectroscopy. *J. Am. Chem. Soc.* **126**, 14239–14248 (2004).
16. Tamura, H. et al. Crystal structures of [Fe]-hydrogenase in complex with inhibitory isocyanides: implications for the H_2-activation site. *Angew. Chem. Int. Ed.* **52**, 9656–9659 (2013).
17. Shima, S. & Ataka, K. Isocyanides inhibit [Fe]-hydrogenase with very high affinity. *FEBS Lett.* **585**, 353–356 (2011).
18. Dey, A. Density functional theory calculations on the mononuclear non-heme iron active site of Hmd hydrogenase: role of the internal ligands in tuning external ligand binding and driving H_2 heterolysis. *J. Am. Chem. Soc.* **132**, 13892–13901 (2010).
19. Hedegård, E. D., Kongsted, J. & Ryde, U. Multiscale modeling of the active site of [Fe] hydrogenase: the H_2 binding site in open and closed protein conformations. *Angew. Chem. Int. Ed.* **54**, 6246–6250 (2015).
20. Yang, X. Z. & Hall, M. B. Monoiron hydrogenase catalysis: hydrogen activation with the formation of a dihydrogen, Fe-H$^{δ-}$–H$^{δ+}$-O, bond and methenyl-H_4MPT^+ triggered hydride transfer. *J. Am. Chem. Soc.* **131**, 10901–10908 (2009).
21. Berkessel, A. Activation of dihydrogen without transition metals. *Curr. Opin. Chem. Biol.* **5**, 486–490 (2001).
22. Berkessel, A. & Thauer, R. K. On the mechanism of catalysis by a metal-free hydrogenase from methanogenic archaea: enzymatic transformation of H_2 without a metal and its analogy to the chemistry of alkanes in superacidic solution. *Angew. Chem. Int. Ed. Engl.* **34**, 2247–2250 (1995).
23. Shima, S., Lyon, E. J., Thauer, R. K., Mienert, B. & Bill, E. Mössbauer studies of the iron–sulfur cluster-free hydrogenase: the electronic state of the mononuclear Fe active site. *J. Am. Chem. Soc.* **127**, 10430–10435 (2005).
24. Korbas, M. et al. The iron–sulfur cluster-free hydrogenase (Hmd) is a metalloenzyme with a novel iron binding motif. *J. Biol. Chem.* **281**, 30804–30813 (2006).
25. Gütlich, P., Bill, E. & Trautwein, A. X. *Mössbauer Spectroscopy and Transition Metal Chemistry* (Springer Verlag, 2011).
26. Chen, D. F., Scopelliti, R. & Hu, X. L. A five-coordinate iron center in the active site of [Fe]-hydrogenase: hints from a model study. *Angew. Chem. Int. Ed.* **50**, 5671–5673 (2011).
27. Shima, S. et al. Reconstitution of [Fe]-hydrogenase using model complexes. *Nat. Chem.* **7**, 995–1002 (2015).
28. Kabsch, W. XDS. *Acta Crystallogr. D* **66**, 125–132 (2010).
29. Winn, M. D. et al. Overview of the CCP4 suite and current developments. *Acta Crystallogr. D* **67**, 235–242 (2011).
30. McCoy, A. J. et al. Phaser crystallographic software. *J. Appl. Crystallogr.* **40**, 658–674 (2007).
31. Emsley, P., Lohkamp, B., Scott, W. G. & Cowtan, K. Features and development of Coot. *Acta Crystallogr. D* **66**, 486–501 (2010).
32. BUSTER version 2.10.1. (Global Phasing, 2016); https://www.globalphasing.com/buster/
33. Adams, P. D. et al. PHENIX: a comprehensive Python-based system for macromolecular structure solution. *Acta Crystallogr. D* **66**, 213–221 (2010).
34. Chen, V. B. et al. MolProbity: all-atom structure validation for macromolecular crystallography. *Acta Crystallogr. D* **66**, 12–21 (2010).
35. Krebs, W. G. & Gerstein, M. The morph server: a standardized system for analyzing and visualizing macromolecular motions in a database framework. *Nucleic Acids Res.* **28**, 1665–1675 (2000).
36. Chung, L. W. et al. The ONIOM method and its applications. *Chem. Rev.* **115**, 5678–5796 (2015).
37. Frisch, M. J. et al. Gaussian 09, Revision D.01 (Gaussian, 2016).
38. Zhao, Y. & Truhlar, D. G. The M06 suite of density functionals for main group thermochemistry, thermochemical kinetics, noncovalent interactions, excited states and transition elements: two new functionals and systematic testing of four M06-class functionals and 12 other functionals. *Theor. Chem. Acc.* **120**, 215–241 (2008).
39. Zhao, Y. & Truhlar, D. G. Density functionals with broad applicability in chemistry. *Acc. Chem. Res.* **41**, 157–167 (2008).

Author contributions

S.S. directed and designed research. G.H. performed cultivation, enzyme purification and crystallization. T.W. and U.E. collected X-ray data. T.W. solved, refined and deposited the structure. M.D.W. and X.H. performed and analysed the QM/MM computations. K.A. performed infrared spectroscopy and E.B. performed Mössbauer spectroscopy. All authors contributed to writing the paper.

Competing interests

The authors declare no competing interests.

Additional information

Supplementary information is available for this paper at https://doi.org/10.1038/s41929-019-0289-4.

Reprints and permissions information is available at www.nature.com/reprints.

Correspondence and requests for materials should be addressed to S.S.

Publisher's note: Springer Nature remains neutral with regard to jurisdictional claims in published maps and institutional affiliations.

© The Author(s), under exclusive licence to Springer Nature Limited 2019

nature research

Corresponding author(s):   Seigo Shima

Last updated by author(s):   Mar 28, 2019

Reporting Summary

Nature Research wishes to improve the reproducibility of the work that we publish. This form provides structure for consistency and transparency in reporting. For further information on Nature Research policies, see Authors & Referees and the Editorial Policy Checklist.

Statistics

For all statistical analyses, confirm that the following items are present in the figure legend, table legend, main text, or Methods section.

n/a	Confirmed	
☒	☐	The exact sample size (n) for each experimental group/condition, given as a discrete number and unit of measurement
☒	☐	A statement on whether measurements were taken from distinct samples or whether the same sample was measured repeatedly
☒	☐	The statistical test(s) used AND whether they are one- or two-sided *Only common tests should be described solely by name; describe more complex techniques in the Methods section.*
☒	☐	A description of all covariates tested
☒	☐	A description of any assumptions or corrections, such as tests of normality and adjustment for multiple comparisons
☒	☐	A full description of the statistical parameters including central tendency (e.g. means) or other basic estimates (e.g. regression coefficient) AND variation (e.g. standard deviation) or associated estimates of uncertainty (e.g. confidence intervals)
☒	☐	For null hypothesis testing, the test statistic (e.g. F, t, r) with confidence intervals, effect sizes, degrees of freedom and P value noted *Give P values as exact values whenever suitable.*
☒	☐	For Bayesian analysis, information on the choice of priors and Markov chain Monte Carlo settings
☒	☐	For hierarchical and complex designs, identification of the appropriate level for tests and full reporting of outcomes
☒	☐	Estimates of effect sizes (e.g. Cohen's d, Pearson's r), indicating how they were calculated

Our web collection on statistics for biologists contains articles on many of the points above.

Software and code

Policy information about availability of computer code

Data collection	All the custom algorithm or software, which is central to the paper, has been reported previously and cited in the manuscript.
Data analysis	All the custom algorithm or software, which is central to the paper, has been reported previously and cited in the manuscript.

For manuscripts utilizing custom algorithms or software that are central to the research but not yet described in published literature, software must be made available to editors/reviewers. We strongly encourage code deposition in a community repository (e.g. GitHub). See the Nature Research guidelines for submitting code & software for further information.

Data

Policy information about availability of data

All manuscripts must include a data availability statement. This statement should provide the following information, where applicable:
- Accession codes, unique identifiers, or web links for publicly available datasets
- A list of figures that have associated raw data
- A description of any restrictions on data availability

The data that support the plots within this paper and other findings of this study are available from the corresponding authors upon reasonable request. X-ray crystallographic data are available in the RCSB-Protein Data Bank under accession numbers 6HAC (Open conformation), 6HAV (Closed conformation Form A) and 6HAE (Closed conformation Form B).

Field-specific reporting

Please select the one below that is the best fit for your research. If you are not sure, read the appropriate sections before making your selection.

☐ Life sciences   ☐ Behavioural & social sciences   ☐ Ecological, evolutionary & environmental sciences

For a reference copy of the document with all sections, see nature.com/documents/nr-reporting-summary-flat.pdf

Life sciences study design

All studies must disclose on these points even when the disclosure is negative.

Sample size	*Describe how sample size was determined, detailing any statistical methods used to predetermine sample size OR if no sample-size calculation was performed, describe how sample sizes were chosen and provide a rationale for why these sample sizes are sufficient.*
Data exclusions	*Describe any data exclusions. If no data were excluded from the analyses, state so OR if data were excluded, describe the exclusions and the rationale behind them, indicating whether exclusion criteria were pre-established.*
Replication	*Describe the measures taken to verify the reproducibility of the experimental findings. If all attempts at replication were successful, confirm this OR if there are any findings that were not replicated or cannot be reproduced, note this and describe why.*
Randomization	*Describe how samples/organisms/participants were allocated into experimental groups. If allocation was not random, describe how covariates were controlled OR if this is not relevant to your study, explain why.*
Blinding	*Describe whether the investigators were blinded to group allocation during data collection and/or analysis. If blinding was not possible, describe why OR explain why blinding was not relevant to your study.*

Behavioural & social sciences study design

All studies must disclose on these points even when the disclosure is negative.

Study description	*Briefly describe the study type including whether data are quantitative, qualitative, or mixed-methods (e.g. qualitative cross-sectional, quantitative experimental, mixed-methods case study).*
Research sample	*State the research sample (e.g. Harvard university undergraduates, villagers in rural India) and provide relevant demographic information (e.g. age, sex) and indicate whether the sample is representative. Provide a rationale for the study sample chosen. For studies involving existing datasets, please describe the dataset and source.*
Sampling strategy	*Describe the sampling procedure (e.g. random, snowball, stratified, convenience). Describe the statistical methods that were used to predetermine sample size OR if no sample-size calculation was performed, describe how sample sizes were chosen and provide a rationale for why these sample sizes are sufficient. For qualitative data, please indicate whether data saturation was considered, and what criteria were used to decide that no further sampling was needed.*
Data collection	*Provide details about the data collection procedure, including the instruments or devices used to record the data (e.g. pen and paper, computer, eye tracker, video or audio equipment) whether anyone was present besides the participant(s) and the researcher, and whether the researcher was blind to experimental condition and/or the study hypothesis during data collection.*
Timing	*Indicate the start and stop dates of data collection. If there is a gap between collection periods, state the dates for each sample cohort.*
Data exclusions	*If no data were excluded from the analyses, state so OR if data were excluded, provide the exact number of exclusions and the rationale behind them, indicating whether exclusion criteria were pre-established.*
Non-participation	*State how many participants dropped out/declined participation and the reason(s) given OR provide response rate OR state that no participants dropped out/declined participation.*
Randomization	*If participants were not allocated into experimental groups, state so OR describe how participants were allocated to groups, and if allocation was not random, describe how covariates were controlled.*

Ecological, evolutionary & environmental sciences study design

All studies must disclose on these points even when the disclosure is negative.

Study description	*Briefly describe the study. For quantitative data include treatment factors and interactions, design structure (e.g. factorial, nested, hierarchical), nature and number of experimental units and replicates.*
Research sample	*Describe the research sample (e.g. a group of tagged Passer domesticus, all Stenocereus thurberi within Organ Pipe Cactus National*

Research sample	*Monument), and provide a rationale for the sample choice. When relevant, describe the organism taxa, source, sex, age range and any manipulations. State what population the sample is meant to represent when applicable. For studies involving existing datasets, describe the data and its source.*
Sampling strategy	*Note the sampling procedure. Describe the statistical methods that were used to predetermine sample size OR if no sample-size calculation was performed, describe how sample sizes were chosen and provide a rationale for why these sample sizes are sufficient.*
Data collection	*Describe the data collection procedure, including who recorded the data and how.*
Timing and spatial scale	*Indicate the start and stop dates of data collection, noting the frequency and periodicity of sampling and providing a rationale for these choices. If there is a gap between collection periods, state the dates for each sample cohort. Specify the spatial scale from which the data are taken*
Data exclusions	*If no data were excluded from the analyses, state so OR if data were excluded, describe the exclusions and the rationale behind them, indicating whether exclusion criteria were pre-established.*
Reproducibility	*Describe the measures taken to verify the reproducibility of experimental findings. For each experiment, note whether any attempts to repeat the experiment failed OR state that all attempts to repeat the experiment were successful.*
Randomization	*Describe how samples/organisms/participants were allocated into groups. If allocation was not random, describe how covariates were controlled. If this is not relevant to your study, explain why.*
Blinding	*Describe the extent of blinding used during data acquisition and analysis. If blinding was not possible, describe why OR explain why blinding was not relevant to your study.*

Did the study involve field work? ☐ Yes ☐ No

Field work, collection and transport

Field conditions	*Describe the study conditions for field work, providing relevant parameters (e.g. temperature, rainfall).*
Location	*State the location of the sampling or experiment, providing relevant parameters (e.g. latitude and longitude, elevation, water depth).*
Access and import/export	*Describe the efforts you have made to access habitats and to collect and import/export your samples in a responsible manner and in compliance with local, national and international laws, noting any permits that were obtained (give the name of the issuing authority, the date of issue, and any identifying information).*
Disturbance	*Describe any disturbance caused by the study and how it was minimized.*

Reporting for specific materials, systems and methods

We require information from authors about some types of materials, experimental systems and methods used in many studies. Here, indicate whether each material, system or method listed is relevant to your study. If you are not sure if a list item applies to your research, read the appropriate section before selecting a response.

Materials & experimental systems

n/a	Involved in the study
☒	☐ Antibodies
☒	☐ Eukaryotic cell lines
☒	☐ Palaeontology
☒	☐ Animals and other organisms
☒	☐ Human research participants
☒	☐ Clinical data

Methods

n/a	Involved in the study
☒	☐ ChIP-seq
☒	☐ Flow cytometry
☒	☐ MRI-based neuroimaging